

PoLaRIS Dataset: A Maritime Object Detection and Tracking Dataset in Pohang Canal

Jiwon Choi^{1*}, Dongjin Cho^{1*}, Gihyeon Lee¹, Hogyun Kim¹, Geonmo Yang¹, Joowan Kim², and Younggun Cho^{1†}

Abstract—Maritime environments often present hazardous situations due to factors such as moving ships or buoys, which become obstacles under the influence of waves. In such challenging conditions, the ability to detect and track potentially hazardous objects is critical for the safe navigation of marine robots. To address the scarcity of comprehensive datasets capturing these dynamic scenarios, we introduce a new multi-modal dataset that includes image and point-wise annotations of maritime hazards. Our dataset provides detailed ground truth for obstacle detection and tracking, including objects as small as 10×10 pixels, which are crucial for maritime safety. To validate the dataset’s effectiveness as a reliable benchmark, we conducted evaluations using various methodologies, including state-of-the-art (SOTA) techniques for object detection and tracking. These evaluations are expected to contribute to performance improvements, particularly in the complex maritime environment. To the best of our knowledge, this is the first dataset offering multi-modal annotations specifically tailored to maritime environments. Our dataset is available at <https://sites.google.com/view/polaris-dataset>.

I. INTRODUCTION

In maritime environments, unmanned surface vehicles (USVs) require precise object recognition to ensure safe autonomous navigation. However, USVs face diverse challenges such as irregular lighting conditions and unpredictable obstacles. Therefore, datasets that account for these factors are crucial for advancing autonomous maritime navigation systems. Although existing maritime datasets [1, 2, 3, 4, 5, 6, 7] have been used as a foundation for USVs navigation research, they suffer from two major limitations.

First, USVs need to accurately detect and track dynamic objects that can disrupt their navigation. However, under limited lighting conditions, such as in cases of light reflection or low visibility [8, 9], RGB cameras are less reliable, making it essential to utilize other sensors beyond the visible spectrum. In addition, precise localization of these obstacles is critical for effective collision avoidance. While multi-sensor data integration is key to addressing these challenges, few datasets comprehensively incorporate such elements.

Second, it is crucial to detect dynamic objects early due to the long stopping distances of USVs. However, existing datasets often lack accurate information on long-range or

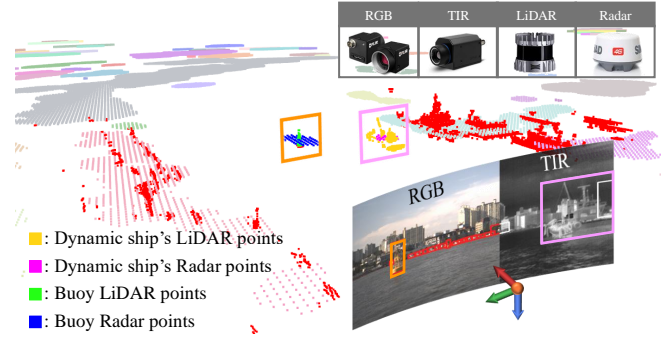


Fig. 1. Pohang00 sequence’s 11194th scene. A clustered sparse Radar point cloud is scattered far and wide in the background. A dense red LiDAR point cloud is also scattered relatively short. To convert this scene PoLaRIS00, we first annotate a RGB image. Then, annotated bounding boxes in the RGB image are mapped to TIR. Finally, we extract only the LiDAR and Radar point clouds projected on annotated bounding boxes of the RGB image to achieve multi-modal annotation.

small objects, particularly in terms of tracking data, which limits their usefulness in real-world scenarios.

As shown in Fig. 1, to address these limitations and support advancements in autonomous maritime navigation, we introduce a new dataset that provides multi-modal object annotations and ground truth for obstacle tracking in USVs operations. The primary contributions of our work are as follows:

- **Multi-Scale Object Annotation:** We offer scale-aware annotations from large to small objects. To streamline this process, we employ an existing object detector to generate initial annotations for large-scale objects, which are then manually refined, along with manual annotation of smaller-scale objects.
- **Dynamic Object Annotation for Tracking:** Our dataset includes tracking data for dynamic objects that may interfere with USV navigation, facilitating more accurate experimentation and improving object detection and tracking performance.
- **Multi-Modal Objects Annotation:** In addition to providing image annotations for Thermal infrared (TIR) data, we offer point-wise annotations for light detection and ranging (LiDAR) and Range Detection and Ranging (Radar) data. These annotations, applicable across different sessions, serve as depth references. To improve efficiency, we employ a semi-automatic labeling approach, which significantly reduces the manual annotation workload while ensuring reliable ground truth through human verification.

^{1*}Jiwon Choi, ^{1*}Dongjin Cho, ¹Gihyeon Lee, ¹Hogyun Kim, ¹Geonmo Yang and ^{1†}Younggun Cho are with the Electrical and Computer Engineering, Inha University, Incheon, South Korea. [jiwon2, d22g66, leekh951, hg.kim, ygm7422]@inha.edu, yg.cho@inha.ac.kr ²Joowan Kim is with the Samsung Heavy Industry, Daejeon, South Korea. joowani.kim@samsung.com (*) represents equal contribution.

TABLE I
VARIOUS MARITIME DATASETS

Datasets	Bounding box				Tracking Annotation			Image size	Session
	Left	Right	TIR	Dynamic	LiDAR	Radar	Image		
USVInland [2]	✗	✗	✗	✗	△	✗	✗	640 × 480	Day
MID [3]	✓	✗	✗	✓	✗	✗	✗	640 × 480	Day
KOLOMVERSE [4]	✓	✗	✗	✗	✗	✗	✗	3840 × 2160	Day/Night
FVessel [10]	✓	✗	✗	✓	✗	✗	✓	2560 × 1440	Day
Singapore [5]	✓	✗	✓	✓	✗	✗	✓	1920 × 1080	Day
Flow [6]	✓	✗	✗	✓	✗	✓	✗	1280 × 720	Day/Night
MODD2 [7]	✓	✓	✗	✗	✗	✗	✗	1278 × 958	Day
Ours	✓	✓	✓	✓	✓	✓	✓	2048 × 1080	Day/Night

△ means that data is provided but label is not provided.

- **Benchmark:** To validate the utility of our dataset as a benchmark, we perform evaluations using conventional and SOTA methods for object detection and tracking. These evaluations confirm the practical applicability of our dataset and demonstrate its potential to drive performance improvements in autonomous navigation systems within complex maritime environments.

The rest of our paper is as follows: Section II introduces related works. Section III represents an overview of our labeling process. Section IV consists of various benchmarks of our datasets. Finally, Section V and Section VI indicate a discussion and a conclusion, respectively.

II. RELATED WORKS

In recent decades, influential datasets and benchmarks have been offered. For instance, *KITTI* dataset [11] provided synchronized multi-modal perception sensors including LiDAR and motion sensor data. *HeLiPR* dataset [12] supplied various types of LiDAR data (e.g. spinning, non-repetitive, and solid-state type). To increase the utility of these impactful datasets, *SemanticKITTI* dataset [13] contributed to the robotics community by presenting segmented point cloud labeling of the *KITTI* dataset [11] and *HeLiMOS* dataset [14] presented diverse LiDAR type’s point cloud labeling of dynamic objects in the *HeLiPR* dataset [12].

Although the number of datasets at maritime is relatively small compared to ground, maritime datasets also have been published as shown in Table I. Cheng et al. [2] released a *USVland* dataset which offers various perception and motion sensors similar to *KITTI* dataset [11]. This dataset allows the testing of algorithms such as simultaneous localization and mapping (SLAM) but did not provide the object-level labeling required for safe navigation. *KOLOMVERSE* [4] and *MID* [3] included many labeled objects under various conditions such as season, weather, and waves. However, it is not suitable for testing real-world navigation-level algorithms such as collision avoidance because it does not provide depth information like LiDAR or Radar. Guo et al. [10] proposed a automatic identification system (AIS) dataset called *FVessel*. This dataset is also not suitable for testing real-world navigation-level algorithms, because it lacks the roll and pitch motions caused by ever-changing waves in the USVs. *MODD2* dataset [7] provided both left and right image labelings, and the *Singapore Maritime* dataset [5]

provided a thermal image labeling along with a RGB image labeling. However, they also didn’t provide the labeled object’s depth information. Cheng et al. [6] provided a *Flow* dataset containing a small object that is approximately 2.5% the size of the image. Although they didn’t provide a 3D bounding box including Radar, they proposed a fusion technique of Radar-vision algorithm to establish a new paradigm for object detection in maritime. However, the lack of a 3D bounding box makes it difficult for users to evaluate the detection algorithm, and the Radar depth is significantly less reliable than LiDAR due to speckle noise and multipath.

To compensate these absences, we propose a *PoLaRIS* presented a multi-modal 3D object’s bounding box with multi-modal depth based on the *Pohang Canal* dataset [1] inspired by the contribution of *SemanticKITTI* [13] and *HeLiMOS* datasets [14]. We also provide a dynamic object, tracking ground truth, and perform various benchmarks.

III. POLARIS DATASET

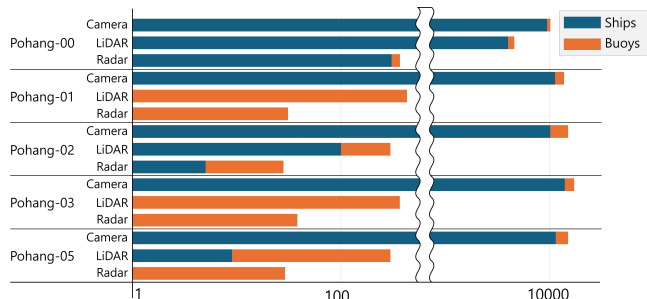


Fig. 2. The vertical axis represents the Pohang00–04 sequences for the sensor modalities: image, LiDAR, and Radar. The horizontal axis indicates the number of labeled data for each sensor modality. *Camera* refers to left, right, and TIR image data, while Radar and LiDAR primarily detect dynamic obstacles and have limitations in identifying distant objects, resulting in significantly fewer data points compared to image data.

Our dataset is based on the *Pohang Canal* dataset [1], which consists of 6 sequences. We selected five major sequences Pohang00, 02, 03, 04 for day and Pohang01 for night. Pohang05 was excluded due to the absence of dynamic objects and poor lighting conditions. These five sequences encompass approximately 360,000 images (e.g., stereo images and TIR) with around 190,000 labels.

Our dataset provides multi-modal information, as shown in Fig. 2, including both static and dynamic object annotations.

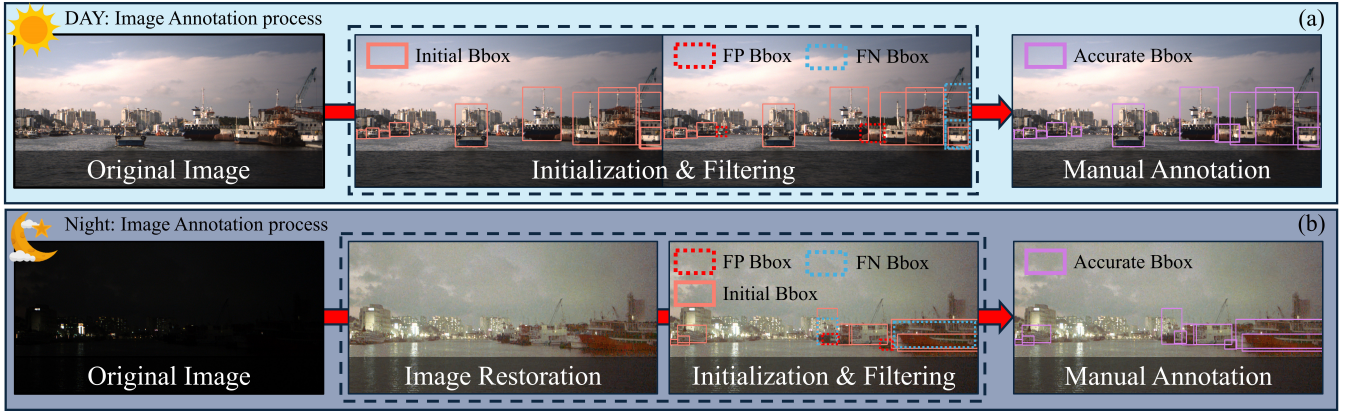


Fig. 3. The process of annotating the left image. (a) shows the annotation process during the day, where objects are more easily detected and labeled. In contrast, (b) illustrates the annotation process at night, requiring additional steps like image restoration due to low visibility. The Initial Bounding box (Bbox) results from the initialization step, while FP and FN Bbox represent false positive and false negative detections, respectively. The Accurate Bbox corresponds to the provided ground truth labels.

It also includes ground truth for small-scale objects, as small as 10×10 pixels (0.0045% of the image size). In addition, we provide tracking ground truth for obstacles, along with depth reference data extracted from ranging sensors, such as LiDAR and Radar.

To streamline the annotation process, we first annotate accurate labels for the left images and use these as references for annotating data from the other sensors.

A. Initial Data Annotation

1) *Left RGB Images*: To ensure precise annotations for the left image of the stereo camera, we perform an initialization process and manual annotation, as shown in Fig. 3. By providing sample bounding boxes via the initialization process, the annotator’s manual labor is exponentially reduced. In this process, we manually sample one image for every 20 images from the entire image set to create a meaningful training set. The remaining images are then used to form the test set, with sample bounding boxes generated using YOLOv8 [15]. Then, a filtering process is applied. Using an Intersection over Union (IoU)-based method, calculated as

$$\text{IoU}(A, B) = \frac{|A \cap B|}{|A \cup B|}, \quad (1)$$

where A and B are initial bounding boxes from the same image, and overlapping boxes are removed if $\text{IoU}(A, B) \geq 0.8$. After the initialization and filtering processes, we manually annotate all small objects that are less than 5% of the total image size (e.g. 2048×1080) in all images.

For **Day** sequence, we assign all the labels for the left image using the initialization process and manual annotation, as shown in Fig. 3-(a).

For **Night** sequence, due to insufficient lighting conditions, it is difficult to distinguish objects in images. To address this limitation, some researchers attempted to use TIR cameras to detect objects [16]. However, annotating precise object labels remains challenging due to the inherent blurring and low resolution of TIR camera outputs. To address this limitation, we utilize restored RGB images for the annotation process, rather than relying on TIR images. For image restoration,

we employ a diffusion-based GSAD approach [17], which represents the SOTA in low-light image enhancement. After that, we manually annotate the restored images, as shown in Fig. 3-(b).

2) *Right RGB Images*: We utilize the ground truth labels from the left image to extract the initial labels of the entire sequences. Since there is a difference in the field of view (FOV) between the left and right cameras, manual annotation is performed to generate ground truth labels for the right camera.

B. Semi-Automatic Annotation

1) *TIR Images*: We leverage extrinsic parameters between TIR camera and left camera for efficient annotation. With the ground truth labels from the left images, it is feasible to obtain the annotation of the TIR camera using the transformation between the two cameras, as shown in the TIR Image Annotation section of Fig. 4-(a).

To briefly explain the two transformations, the bounding box corner in the TIR image is followed as:

$$bb_t = K_t \cdot T_l^t \cdot K_l^{-1} \cdot bb_l, \quad (2)$$

where T_l^t is the transformation between the TIR and left cameras, bb represents the bounding box corner (e.g. $[u \ v \ 1]^T$), and K is the camera’s intrinsic matrix, with subscripts t and l indicating the TIR and left cameras

The converted bounding box is used as the reference label for TIR image. However, due to transformation errors and FOV differences between sensors, post-processing on the reference label is necessary. For this purpose, we need to distinguish the object, but TIR images are inevitably a 16-bit. Therefore, to address this, we used Fieldscale [18] to convert the 16-bit TIR image to 8-bit for improved visualization, and then applied manual annotations to ensure accurate labeling. This process is demonstrated in the manual annotations section shown in the TIR Image Annotation section of Fig. 4-(a).

2) *LiDAR Points*: We generate point-wise annotations for LiDAR sensor data on obstacles, based on the accurate label information from the left image. First, we project the LiDAR

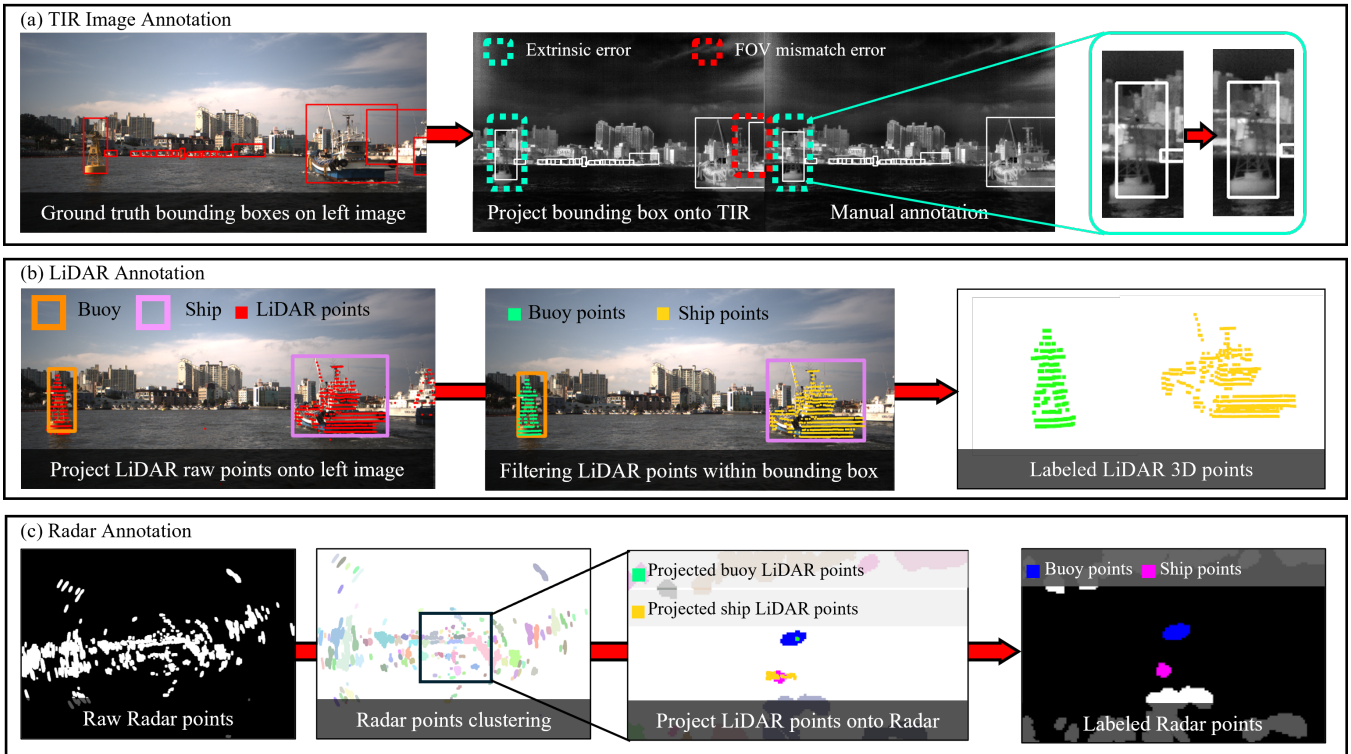


Fig. 4. The process of semi-automatic annotation for multi-modal sensors. (a) shows the process of defining labels in the TIR image using transformation data from the left image and manually correcting label errors. (b) shows the process of filtering LiDAR points based on the ground truth labels from the left image to obtain LiDAR points’ annotation. (c) demonstrates the process of clustering Radar points and defining their labels by identify clusters that overlap with the labeled points obtained in (b).

points onto the left image based on the transformation between the left camera and LiDAR. Then, we remove all projected LiDAR points outside the bounding box in the left image, as demonstrated in the LiDAR Annotation section of Fig. 4-(b). However, the rectangular bounding box does not perfectly match the object’s shape, some non-object areas may be included. As a result, defining point labels based on the bounding box can lead to false positives. To enhance accuracy, we manually verify and remove points within the bounding box that do not belong to the object. This process ensures that the 3D point labels more accurately represent the object’s shape and position.

3) *Radar Points*: It is difficult to directly fuse the camera and Radar to generate annotations because the camera captures 2D forward-view images, while Radar collects data in a 2D bird’s-eye view (BEV) format. To overcome this limitation, we fuse the Radar with LiDAR, which provides 3D information, instead of directly using the camera. Then, we generate point-wise Radar annotations for dynamic objects, based on the existing LiDAR annotations as shown in the Radar Annotation section of Fig. 4-(c). The process for point-wise annotation of Radar consists of the following steps:

- 1) Convert the labeled LiDAR points to Radar coordinates, and project them in BEV format.
- 2) Identify the overlap region between the projected annotation LiDAR points and the Radar data in 3D space. Due to the wide horizontal beamwidth of the marine radar sensor [19], it is not possible to assign point-

wise annotations to areas that overlap with the LiDAR points.

- 3) Apply the DBSCAN [20] algorithm to cluster the Radar data, and assign point-wise annotation to the Radar clusters that overlap with the labeled LiDAR points.

This process reflects the characteristics of the Radar sensor and contributes to improving annotation accuracy.

C. Dynamic Object Tracking

In our dataset, dynamic objects (e.g. moving ships and buoys) are defined as obstacles. Then, they are assigned unique identifiers (IDs) during the tracking process.

We aim to provide tracking ground truth for multi-scale objects. Therefore, we generate tracking ground truth from

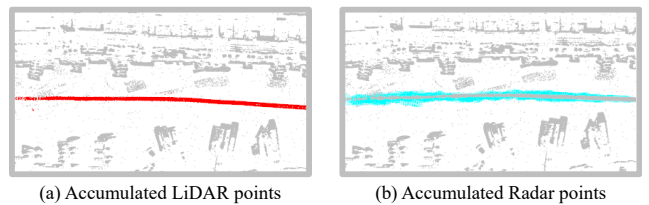


Fig. 5. Illustration of dynamic objects.

the moment of the stage of object detection, even for dynamic objects as small as 10×10 pixels. By providing tracking ground truth data for small, distant, and obscured objects, our dataset can validate experiments on objects of various

sizes. To verify this, several evaluations are conducted in Section IV.

In addition, by combining 2D tracking ground truth with the 3D labeled points from both LiDAR and Radar, we can provide precise metrics as shown in Fig. 5.

D. File Structure

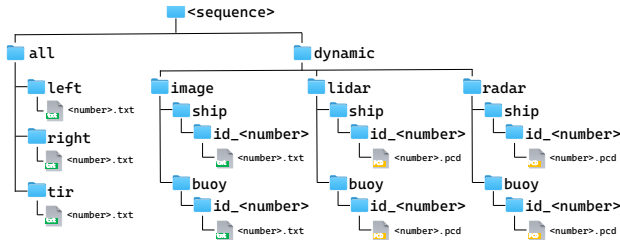


Fig. 6. File structure of our dataset.

All label files for the image sensors are stored in a folder named *all*. The image labels and point-wise labels of dynamic objects are stored in the *dynamic* folder, as shown in Fig. 6.

IV. BENCHMARKS

To demonstrate validity for object detection and tracking across various modalities and lighting conditions, we conducted tests in the Pohang00 sequence, which contains the highest number of multi-dynamic objects. For evaluation in low-light conditions and scenarios involving single-dynamic objects, we utilized the Pohang01 sequence. Several metrics were used to assess performance on sequences containing obstacles. All scenarios utilized RGB and TIR images for detection and tracking evaluations, with TIR images converted to 8-bit using SOTA methods from Fieldscale [18]. For detection evaluations, we sampled 5% of images from each of Regions (a)-(d) in Fig. 7 for training and the rest for test sets. All detection results were fixed, and we evaluated the performance of the trackers using YOLOv8 [15].

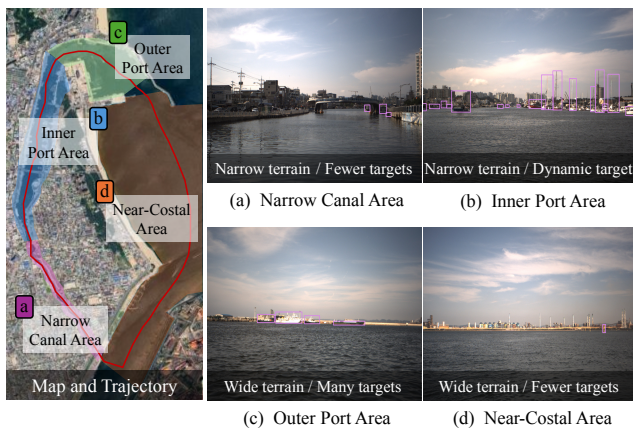


Fig. 7. The Pohang dataset [1] trajectory is shown, divided into four regions: Narrow Canal Area, Inner Port Area, Outer Port Area, and Near-Coastal Area. Regions (b) and (c) contain more objects compared to Regions (a) and (d).

A. Evaluation Metrics

1) *mAP*: The performance of the object detection model was evaluated using the Mean Average Precision (mAP), which is calculated based on precision and recall:

$$\text{Precision} = \frac{\text{TP}}{\text{TP} + \text{FP}}, \quad \text{Recall} = \frac{\text{TP}}{\text{TP} + \text{FN}}, \quad (3)$$

$$\text{AP} = \int_0^1 p(r) dr, \quad (4)$$

where TP, FP, and FN represent true positives, false positives, and false negatives. The Average Precision (Average Precision (AP)) is defined as the area under the precision-recall curve, where $p(r)$ denotes the precision at a given recall r .

$$\text{mAP} = \frac{1}{N} \sum_{i=1}^N \text{AP}_i, \quad (5)$$

The mAP is then computed as the mean of the AP values across all classes, where N is the total number of classes, and AP_i is the Average Precision for class i .

2) *MOTA*: The Multiple Object Tracking Accuracy Multiple Object Tracking Accuracy (MOTA) [21] is a standard metric used to evaluate the performance of tracking algorithms. It combines three types of errors: FP, FN, and identity switches (IDSW). MOTA is defined as follows:

$$\text{MOTA} = 1 - \frac{|FN| + |FP| + |IDSW|}{|gtDet|}, \quad (6)$$

where $|FN|$ represents the number of missed detections, $|FP|$ represents the number of incorrect detections, and $|IDSW|$ is the number of identity switches. $|gtDet|$ is the total number of ground truth detections. This metric penalizes tracking errors, with a higher MOTA indicating better tracking performance.

3) *IDF1*: The IDF1 score [22] measures the accuracy of the predicted trajectories in terms of identity preservation. It evaluates how well the tracker assigns the correct identity to each object throughout the video sequence. The IDF1 score is defined as:

$$\text{IDF1} = \frac{2 \times \text{IDTP}}{2 \times \text{IDTP} + \text{IDFP} + \text{IDFN}}, \quad (7)$$

where IDTP , IDFP , and IDFN represent identity true positives, false positives, and false negatives, respectively. The IDF1 metric focuses on identity-based accuracy, providing insights into the effectiveness of the tracking system in maintaining object identities over time.

Additionally, ID Precision (IDP) and ID Recall (IDR) are used to evaluate identity assignment performance:

$$\text{IDP} = \frac{\text{IDTP}}{\text{IDTP} + \text{IDFP}}, \quad \text{IDR} = \frac{\text{IDTP}}{\text{IDTP} + \text{IDFN}} \quad (8)$$

IDP measures the precision of identity assignments, while IDR measures the recall of the identity assignments.

B. Experimental Settings

All models were trained using the AdamW [27] optimizer (learning rate: 0.000714, momentum: 0.9) on an NVIDIA

TABLE II
EVALUATION - OBJECT DETECTION

Method	Pre-train	Pohang00 (Day-RGB)			Pohang01 (Night-RGB)			Pohang00 (Day-TIR)			Pohang01 (Night-TIR)		
		mAP↑ (%)	Ship	Buoy	mAP↑ (%)	Ship	Buoy	mAP↑ (%)	Ship	Buoy	mAP↑ (%)	Ship	Buoy
YOLOv8-L	X	78.0	89.3	66.6	77.2	88.4	66.0	58.4	70.1	46.7	64.0	71.6	56.5
YOLOv8-L	COCO	79.6	91.0	68.1	84.2	91.3	77.1	-	-	-	-	-	-
YOLOv10-L	X	75.6	87.6	63.5	72.4	85.9	58.9	54.9	66.3	43.6	59.1	69.0	49.3
YOLOv10-L	COCO	80.1	90.6	69.6	82.9	90.9	74.9	-	-	-	-	-	-
RT-DETR-R50	X	78.4	86.7	70.0	69.1	77.6	60.7	53.4	60.9	45.9	55.2	62.1	48.3
YOLO-World-L w/o training	O+G	1.5	2.8	0.2	0.7	1.1	0.0	-	-	-	-	-	-
Grounding Dino w/o training	O+G+C	2.3	4.3	0.3	0.7	1.4	0.0	-	-	-	-	-	-

'O', 'G', and 'C' denote pertaining using Objects365 [23], GoldG [24, 25], and Cap4M [26] dataset.

GeForce RTX 3090 GPU. From the Pohang00 (during the day) and Pohang01 (during the night) sequences, 2,158 and 2,399 images were sampled for training, and 959 and 1,066 images for validation, respectively.

C. Object Detection

1) *Implementation Details*: We evaluated object detection models using SOTA methods from both the You Only Look Once (YOLO) and Detection Transformer (DETR) series. Specifically, we employed YOLOv8 [15], YOLOv10 [28], and RT-DETR [29] as closed-set models, alongside open-set models like YOLO-World [30] and Grounding DINO [26] to assess the generalization capabilities of our dataset. For YOLOv8 [15] and YOLOv10 [28], RGB images were resized to 736×736 , and TIR images to 512×512 . Due to the modality differences between TIR and RGB images, we did not use models pre-trained on the COCO [31] dataset for TIR experiments.

2) *Detection Results*: Table II summarizes the performance of the models trained on RGB and TIR images under varying lighting conditions, reporting mAP scores over IoU thresholds ranging from 0.50 to 0.95. In RGB-based detection, the models exhibited strong performance in the Ship class, with significant improvements in the nighttime Buoy class after COCO pre-training. However, the performance in TIR-based detection was comparatively lower, likely because the model was optimized for RGB images. The open vocabulary models exhibited generally lower performance, which can be attributed to the challenging nature of the dataset, containing a large number of small objects.

D. Object Tracking

1) *Implementation Details*: We evaluated the performance of the tracker on dynamic objects using heuristic-based multi object tracking methods, including SORT [32], ByteTrack [33], OC-SORT [34], and Hybrid-SORT [35]. All tracker experiments, YOLOv8-L (as presented in Table II) was used as the detection model, with the IoU threshold fixed at 0.3. To evaluate performance, we used the MOTA and IDF1 metrics to assess accuracy and ID matching.

2) *Tracking Results*: Table III validates the object tracking methodology using RGB and TIR sensors in varying illumination conditions. While RGB-based trackers perform well day and night, TIR-based trackers underperform compared to RGB. In addition, OC-SORT tracker performed better in the multi-dynamic objects sequence(Pohang00), while ByteTrack performed better in the single-dynamic objects

TABLE III
EVALUATION - OBJECT TRACKING

Data	sensor	Method	MOTA↑	IDR↑	IDP↑	IDF1↑
Pohang00	RGB	SORT	90.9%	99.9%	91.1%	95.3%
		ByteTrack	96.0%	99.7%	96.3%	98.0%
		OC-SORT	98.5%	99.8%	98.6%	99.2%
		Hybrid-SORT	97.8%	99.8%	97.9%	98.9%
Pohang01	RGB	SORT	85.0%	99.8%	85.1%	91.9%
		ByteTrack	99.6%	99.8%	99.8%	99.8%
		OC-SORT	99.3%	99.9%	99.4%	99.7%
		Hybrid-SORT	98.2%	99.9%	98.2%	99.1%
Pohang00	TIR	SORT	62.5%	97.9%	63.9%	77.4%
		ByteTrack	71.9%	97.7%	73.7%	84.0%
		OC-SORT	75.5%	97.7%	77.4%	86.4%
		Hybrid-SORT	74.8%	97.7%	76.6%	85.9%
Pohang01	TIR	SORT	71.3%	94.0%	76.1%	84.1%
		ByteTrack	88.0%	94.0%	94.0%	94.0%
		OC-SORT	82.5%	93.1%	89.2%	91.1%
		Hybrid-SORT	81.6%	93.0%	88.2%	90.6%

sequence(Pohang01). These results confirm that the dataset is valid for multi-sensor object tracking tasks.

V. CONCLUSION & DISCUSSION

In this paper, we introduced POLARIS, a multi-modal dataset designed for object labeling in maritime environments. The dataset includes approximately 360,000 labeled images from RGB and TIR cameras, along with point-wise annotations from Radar and LiDAR. Tracking ground truths for dynamic objects are also provided, projected within bounding boxes, enabling the evaluation of detection and tracking algorithms.

One of the key challenges in maritime environments is the variability in object sizes and sensor ranges. POLARIS addresses this by offering detailed multi-modal annotations to improve navigation and object detection in dynamic maritime settings. In future work, we will extend the dataset to cover more diverse environments and introduce semantic-level annotations alongside bounding box-level annotations to enhance its utility further.

VI. ACKNOWLEDGEMENTS

We appreciate Prof. Jinhwan Kim's *MORIN* group, particularly Dongha Chung, for publishing the *Pohang Canal* dataset [1].

REFERENCES

- [1] D. Chung, J. Kim, C. Lee, and J. Kim, "Pohang canal dataset: A multimodal maritime dataset for autonomous navigation in restricted waters," *The International Journal of Robotics Research*, vol. 42, no. 12, pp. 1104–1114, 2023.
- [2] Y. Cheng, M. Jiang, J. Zhu, and Y. Liu, "Are we ready for unmanned surface vehicles in inland waterways? the usv inland multisensor dataset and benchmark," *IEEE Robotics and Automation Letters*, vol. 6, no. 2, pp. 3964–3970, 2021.

- [3] J. Liu, H. Li, J. Luo, S. Xie, and Y. Sun, "Efficient obstacle detection based on prior estimation network and spatially constrained mixture model for unmanned surface vehicles," *Journal of Field Robotics*, vol. 38, no. 2, pp. 212–228, 2021.
- [4] A. Nanda, S. W. Cho, H. Lee, and J. H. Park, "Kolomverse: Kriso open large-scale image dataset for object detection in the maritime universe," *arXiv preprint arXiv:2206.09885*, 2022.
- [5] D. K. Prasad, D. Rajan, L. Rachmawati, E. Rajabally, and C. Quek, "Video processing from electro-optical sensors for object detection and tracking in a maritime environment: A survey," *IEEE Transactions on Intelligent Transportation Systems*, vol. 18, no. 8, pp. 1993–2016, 2017.
- [6] Y. Cheng, J. Zhu, M. Jiang, J. Fu, C. Pang, P. Wang, K. Sankaran, O. Onabola, Y. Liu, D. Liu, and Y. Bengio, "Flow: A dataset and benchmark for floating waste detection in inland waters," in *Proceedings of the IEEE/CVF International Conference on Computer Vision (ICCV)*, October 2021, pp. 10953–10962.
- [7] B. Bovcon, J. Muhovič, J. Perš, and M. Kristan, "The mastr1325 dataset for training deep usv obstacle detection models," in *2019 IEEE/RSJ International Conference on Intelligent Robots and Systems (IROS)*. IEEE, 2019, pp. 3431–3438.
- [8] A. A. AlMansoori, I. Swamidoss, S. Sayadi, and A. Almarzooqi, "Analysis of different tracking algorithms applied on thermal infrared imagery for maritime surveillance systems," in *Artificial Intelligence and Machine Learning in Defense Applications II*, vol. 11543. SPIE, 2020, pp. 30–40.
- [9] M. M. Zhang, J. Choi, K. Daniilidis, M. T. Wolf, and C. Kanan, "Vais: A dataset for recognizing maritime imagery in the visible and infrared spectrums," in *Proceedings of the IEEE conference on computer vision and pattern recognition workshops*, 2015, pp. 10–16.
- [10] Y. Guo, R. W. Liu, J. Qu, Y. Lu, F. Zhu, and Y. Lv, "Asynchronous trajectory matching-based multimodal maritime data fusion for vessel traffic surveillance in inland waterways," *IEEE Transactions on Intelligent Transportation Systems*, vol. 24, no. 11, pp. 12 779–12 792, 2023.
- [11] A. Geiger, P. Lenz, and R. Urtasun, "Are we ready for autonomous driving? the kitti vision benchmark suite," in *2012 IEEE conference on computer vision and pattern recognition*. IEEE, 2012, pp. 3354–3361.
- [12] M. Jung, W. Yang, D. Lee, H. Gil, G. Kim, and A. Kim, "Helipr: Heterogeneous lidar dataset for inter-lidar place recognition under spatiotemporal variations," *The International Journal of Robotics Research*, p. 02783649241242136, 2023.
- [13] J. Behley, M. Garbade, A. Milioto, J. Quenzel, S. Behnke, C. Stachniss, and J. Gall, "Semantickitti: A dataset for semantic scene understanding of lidar sequences," in *Proceedings of the IEEE/CVF international conference on computer vision*, 2019, pp. 9297–9307.
- [14] H. Lim, S. Jang, B. Mersch, J. Behley, H. Myung, and C. Stachniss, "Helimos: A dataset for moving object segmentation in 3d point clouds from heterogeneous lidar sensors," *arXiv preprint arXiv:2408.06328*, 2024.
- [15] G. Jocher, A. Chaurasia, and J. Qiu, "Ultralytics yolov8," 2023, version 8.0.0. [Online]. Available: <https://github.com/ultralytics/ultralytics>
- [16] M. Krišto, M. Ivasic-Kos, and M. Pobar, "Thermal object detection in difficult weather conditions using yolo," *IEEE access*, vol. 8, pp. 125 459–125 476, 2020.
- [17] J. Hou, Z. Zhu, J. Hou, H. Liu, H. Zeng, and H. Yuan, "Global structure-aware diffusion process for low-light image enhancement," *Advances in Neural Information Processing Systems*, vol. 36, 2024.
- [18] H. Gil, M.-H. Jeon, and A. Kim, "Fieldscale: Locality-aware field-based adaptive rescaling for thermal infrared image," *IEEE Robotics and Automation Letters*, 2024.
- [19] A. G. Bole, A. D. Wall, and A. Norris, *Radar and ARPA manual: radar, AIS and target tracking for marine radar users*. Butterworth-Heinemann, 2013.
- [20] M. Ester, H.-P. Kriegel, J. Sander, X. Xu *et al.*, "A density-based algorithm for discovering clusters in large spatial databases with noise," in *kdd*, vol. 96, no. 34, 1996, pp. 226–231.
- [21] K. Bernardin and R. Stiefelwagen, "Evaluating multiple object tracking performance: the clear mot metrics," *EURASIP Journal on Image and Video Processing*, vol. 2008, pp. 1–10, 2008.
- [22] E. Ristani, F. Solera, R. Zou, R. Cucchiara, and C. Tomasi, "Performance measures and a data set for multi-target, multi-camera tracking," in *European conference on computer vision*. Springer, 2016, pp. 17–35.
- [23] S. Shao, Z. Li, T. Zhang, C. Peng, G. Yu, X. Zhang, J. Li, and J. Sun, "Objects365: A large-scale, high-quality dataset for object detection," in *Proceedings of the IEEE/CVF international conference on computer vision*, 2019, pp. 8430–8439.
- [24] D. A. Hudson and C. D. Manning, "Gqa: A new dataset for real-world visual reasoning and compositional question answering," in *Proceedings of the IEEE/CVF conference on computer vision and pattern recognition*, 2019, pp. 6700–6709.
- [25] B. A. Plummer, L. Wang, C. M. Cervantes, J. C. Caicedo, J. Hockenmaier, and S. Lazebnik, "Flickr30k entities: Collecting region-to-phrase correspondences for richer image-to-sentence models," in *Proceedings of the IEEE international conference on computer vision*, 2015, pp. 2641–2649.
- [26] S. Liu, Z. Zeng, T. Ren, F. Li, H. Zhang, J. Yang, C. Li, J. Yang, H. Su, J. Zhu *et al.*, "Grounding dino: Marrying dino with grounded pre-training for open-set object detection," *arXiv preprint arXiv:2303.05499*, 2023.
- [27] I. Loshchilov, "Decoupled weight decay regularization," *arXiv preprint arXiv:1711.05101*, 2017.
- [28] A. Wang, H. Chen, L. Liu, K. Chen, Z. Lin, J. Han, and G. Ding, "Yolov10: Real-time end-to-end object detection," *arXiv preprint arXiv:2405.14458*, 2024.
- [29] Y. Zhao, W. Lv, S. Xu, J. Wei, G. Wang, Q. Dang, Y. Liu, and J. Chen, "Detrs beat yolos on real-time object detection," in *Proceedings of the IEEE/CVF Conference on Computer Vision and Pattern Recognition*, 2024, pp. 16 965–16 974.
- [30] T. Cheng, L. Song, Y. Ge, W. Liu, X. Wang, and Y. Shan, "Yolo-world: Real-time open-vocabulary object detection," *arXiv preprint arXiv:2401.17270*, 2024.
- [31] T.-Y. Lin, M. Maire, S. Belongie, J. Hays, P. Perona, D. Ramanan, P. Dollár, and C. L. Zitnick, "Microsoft coco: Common objects in context," in *Computer Vision—ECCV 2014: 13th European Conference, Zurich, Switzerland, September 6–12, 2014, Proceedings, Part V 13*. Springer, 2014, pp. 740–755.
- [32] A. Bewley, Z. Ge, L. Ott, F. Ramos, and B. Upcroft, "Simple online and realtime tracking," in *2016 IEEE international conference on image processing (ICIP)*. IEEE, 2016, pp. 3464–3468.
- [33] Y. Zhang, P. Sun, Y. Jiang, D. Yu, F. Weng, Z. Yuan, P. Luo, W. Liu, and X. Wang, "Bytetrack: Multi-object tracking by associating every detection box," in *European conference on computer vision*. Springer, 2022, pp. 1–21.
- [34] J. Cao, J. Pang, X. Weng, R. Khrodgar, and K. Kitani, "Observation-centric sort: Rethinking sort for robust multi-object tracking," in *Proceedings of the IEEE/CVF conference on computer vision and pattern recognition*, 2023, pp. 9686–9696.
- [35] M. Yang, G. Han, B. Yan, W. Zhang, J. Qi, H. Lu, and D. Wang, "Hybrid-sort: Weak cues matter for online multi-object tracking," in *Proceedings of the AAAI Conference on Artificial Intelligence*, vol. 38, no. 7, 2024, pp. 6504–6512.